View metadata, citation and similar papers at core.ac.uk
brought to you by CORE
provided by Tomsk State University Repository

ISSN 1810-2328, Journal of Engineering Thermophysics, 2015, Vol. 24, No. 1, pp. 22–32. © Pleiades Publishing, Ltd., 2015.

Numerical Analysis of 3D Regimes of Natural Convection and Surface Radiation in a Differentially Heated Enclosure

S. G. Martyushev[1] and M. A. Sheremet[1,2*]

[1] *Tomsk State University, pr. Lenina 36, Tomsk, 634050 Russia*

[2] *Tomsk Polytechnic University, pr. Lenina 30, Tomsk, 634050 Russia*

Received February 6, 2013

Abstract—Numerical analysis of 3D regimes of convection-radiation heat transfer in cubic enclosure with two isothermal faces and adiabatic walls is performed. The mathematical model is constructed in dimensionless variables "vector potential–vorticity vector–temperature" in the Boussinesq approximation and with regard to diathermal medium filling the enclosure. 3D temperature and velocity fields, medium motion trajectories in a wide range of key parameters are obtained. Correlations for the integral heat exchange coefficient as a function of the key process characteristics are found.

DOI: 10.1134/S1810232815010038

INTRODUCTION

Development of state-of-the-art electronics is associated with constant increase of efficiency of the products and reduction of their mass-dimension parameters. Such tendencies lead to rapid increase in the dissipated heat power. For this reason, in designing electronics it is particularly important to develop methods of heat removal and temperature control [1, 2]. It is known that in air-filled enclosures the intensity of heat transfer as a result of convection is comparable with that of radiation energy transfer [3, 4]. In relation to the last-mentioned fact, it seems most urgent to simultaneously analyze the processes of energy transfer by mechanisms of convection and radiation in enclosures and thus to find the most common regularities of combined heat exchange.

By present, few theoretical investigations of the convection-radiation heat transfer in enclosures have been carried out [5–10], which is concerned with substantial computational expenses and mathematical complications. Three-dimensional convection and radiation in a cubic cavity filled with diathermal or nontransparent media were numerically analyzed in [5]. The mathematical model formulated in primitive variables was implemented by the control volume method with the use of the discrete ordinate method for solving the radiation transfer equation. As a result, it was found that the heat flux density substantially grows in the case of a radiation-transmitting medium due to the radiation component of the process. In investigation of a nontransparent medium it was shown that for a fixed value of optical medium thickness an increase in the Rayleigh number leads to an increase in the heat flux density, and an increase of τ_λ reduces the heat flux. As a result of mathematical modeling of hydrodynamics and heat transfer due to mechanisms of combined convection, thermal radiation, and heat conductivity in a cubic enclosure exposed to external flow it was shown [6] that thermal radiation may have the governing value in formation of a temperature field. An increase in the Reynolds number of the external incoming flow results in a change of the Nusselt number and leads to decreasing average temperature of the cubic cavity. Numerical analysis of the effect of surface radiation on 3D regimes in a differentially heated parallelepiped at $\mathrm{Pr} = 13.6$ and $\mathrm{Ra} = 10^6$ has shown the presence of relative intense spiral motion in the volume [7]. As a result of mathematical modeling of natural convection in a shallow wedge with a small aperture angle subject to solar radiation [8], there were found three independent stages of development of convection recirculation: an initial stage (dominance of heat conductivity and

* E-mail: Michael-sher@yandex.ru

formation of thermal boundary layer), a transition stage (formation of Benar instability) and a quasi-stationary stage (formation of a steady-state temperature field and reduction of instability intensity). The numerically found effects were previously observed in the experiment of [9]. Mathematical modeling of conjugate natural convection in an enclosure with regard to thermal radiation in the Rosseland approximation [10] has made it possible to reveal a temperature growth in a cavity on the initial time interval by 11% on average. It was also shown that increasing thermal conductivity coefficient of the material of solid walls results in decreasing integral heat transfer coefficient on the surface of the energy source.

The aim of the present work is mathematical modeling of 3D regimes of thermal gravitational convection and surface radiation in a cubic enclosure filled with diathermal medium Pr = 0.7 in the presence of two vertical isothermal faces. Comparison of the obtained results with the data on the 2D model makes it possible to evaluate the 3D statement for a cubic cavity.

STATEMENT OF THE PROBLEM

We consider the combined natural convection–surface radiation process in a cubic enclosure (see Fig. 1). It is assumed that initially the walls of the enclosure and the air that fills it have a constant temperature that is the same at all points, the air being stagnant. The vertical walls ($x = 0,\ x = L$) of the enclosure are assumed to be isothermal with temperatures $T_\mathrm{h} > T_\mathrm{c}$, and the rest of the walls are adiabatic. The air is assumed to be a Newtonian incompressible diathermal medium satisfying the Boussinesq approximation. It is assumed that all cube faces are diffusive-gray radiators. For the reflected radiation, there are two assumptions [11]: the reflected radiation is diffusive, i.e., the reflected radiation intensity at any point of the surface boundary is uniformly distributed in all directions, and the reflected radiation is uniformly distributed over each surface of the closed solution domain.

In this statement, the heat transfer process is described by a system of nonstationary 3D equations of convection in the Boussinesq approximation in the enclosure [10, 12]. The mathematical model is formulated in dimensionless variables "vector potential–vorticity vector–temperature."

The distance scale was the size of solution domain L. To obtain a dimensionless form of the system of equations, we used the following relationships:

$$X = x/L,\ Y = y/L,\ Z = z/L,\ \tau = t/t_0,\ U = u/V_0,\ V = v/V_0,\ W = w/V_0,$$
$$\Theta = (T - T_0)/(T_\mathrm{h} - T_\mathrm{c}),\ \Psi_x = \psi_x/\psi_0,\ \Psi_y = \psi_y/\psi_0,\ \Psi_z = \psi_z/\psi_0,$$
$$\Omega_x = \omega_x/\omega_0,\ \Omega_y = \omega_y/\omega_0,\ \Omega_z = \omega_z/\omega_0,\ \omega_0 = V_0/L,\ \psi_0 = V_0 L,$$
$$V_0 = \sqrt{g_z\beta(T_\mathrm{h} - T_\mathrm{c})L},\ t_0 = L/V_0 = [L/(g_z\beta(T_\mathrm{h} - T_\mathrm{c}))]^{0.5}.$$

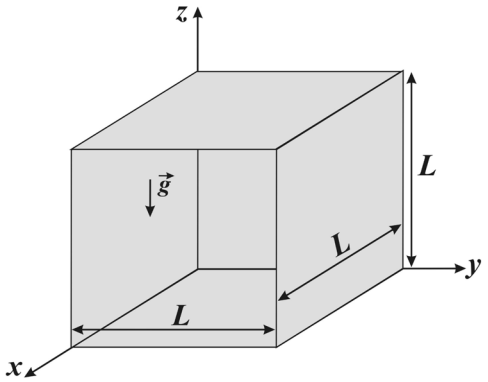

Fig. 1. Solution domain of the problem considered.

Dimensionless heat transfer equations:

$$\frac{\partial \Omega_x}{\partial \tau} + U\frac{\partial \Omega_x}{\partial X} + V\frac{\partial \Omega_x}{\partial Y} + W\frac{\partial \Omega_x}{\partial Z} - \Omega_x\frac{\partial U}{\partial X} - \Omega_y\frac{\partial U}{\partial Y} - \Omega_z\frac{\partial U}{\partial Z} = \sqrt{\frac{\mathrm{Pr}}{\mathrm{Ra}}}\left(\frac{\partial^2 \Omega_x}{\partial X^2} + \frac{\partial^2 \Omega_x}{\partial Y^2} + \frac{\partial^2 \Omega_x}{\partial Z^2}\right) + \frac{\partial \Theta}{\partial Y}, \tag{1}$$

$$\frac{\partial \Omega_y}{\partial \tau} + U\frac{\partial \Omega_y}{\partial X} + V\frac{\partial \Omega_y}{\partial Y} + W\frac{\partial \Omega_y}{\partial Z} - \Omega_x\frac{\partial V}{\partial X} - \Omega_y\frac{\partial V}{\partial Y} - \Omega_z\frac{\partial V}{\partial Z} = \sqrt{\frac{\mathrm{Pr}}{\mathrm{Ra}}}\left(\frac{\partial^2 \Omega_y}{\partial X^2} + \frac{\partial^2 \Omega_y}{\partial Y^2} + \frac{\partial^2 \Omega_y}{\partial Z^2}\right) - \frac{\partial \Theta}{\partial X}, \tag{2}$$

$$\frac{\partial \Omega_z}{\partial \tau} + U\frac{\partial \Omega_z}{\partial X} + V\frac{\partial \Omega_z}{\partial Y} + W\frac{\partial \Omega_z}{\partial Z} - \Omega_x\frac{\partial W}{\partial X} - \Omega_y\frac{\partial W}{\partial Y} - \Omega_z\frac{\partial W}{\partial Z} = \sqrt{\frac{\mathrm{Pr}}{\mathrm{Ra}}}\left(\frac{\partial^2 \Omega_z}{\partial X^2} + \frac{\partial^2 \Omega_z}{\partial Y^2} + \frac{\partial^2 \Omega_z}{\partial Z^2}\right), \tag{3}$$

$$\frac{\partial^2 \Psi_x}{\partial X^2} + \frac{\partial^2 \Psi_x}{\partial Y^2} + \frac{\partial^2 \Psi_x}{\partial Z^2} = -\Omega_x, \tag{4}$$

$$\frac{\partial^2 \Psi_y}{\partial X^2} + \frac{\partial^2 \Psi_y}{\partial Y^2} + \frac{\partial^2 \Psi_y}{\partial Z^2} = -\Omega_y, \tag{5}$$

$$\frac{\partial^2 \Psi_z}{\partial X^2} + \frac{\partial^2 \Psi_z}{\partial Y^2} + \frac{\partial^2 \Psi_z}{\partial Z^2} = -\Omega_z, \tag{6}$$

$$\frac{\partial \Theta}{\partial \tau} + U\frac{\partial \Theta}{\partial X} + V\frac{\partial \Theta}{\partial Y} + W\frac{\partial \Theta}{\partial Z} = \frac{1}{\sqrt{\mathrm{Ra}\cdot\mathrm{Pr}}}\left(\frac{\partial^2 \Theta}{\partial X^2} + \frac{\partial^2 \Theta}{\partial Y^2} + \frac{\partial^2 \Theta}{\partial Z^2}\right). \tag{7}$$

Initial conditions for the system of equations (1)–(7):

$$\Psi_x(X,Y,Z,0) = \Psi_y(X,Y,Z,0) = \Psi_z(X,Y,Z,0) = 0,$$
$$\Omega_x(X,Y,Z,0) = \Omega_y(X,Y,Z,0) = \Omega_z(X,Y,Z,0) = \Theta(X,Y,Z,0) = 0.$$

Boundary conditions:

at the boundary $X = 0$: $\frac{\partial \Psi_x}{\partial X} = \Psi_y = \Psi_z = 0$, $\Theta = 0.5$;

at the boundary $X = 1$: $\frac{\partial \Psi_x}{\partial X} = \Psi_y = \Psi_z = 0$, $\Theta = -0.5$;

at boundaries $Y = 0$ and $Y = 1$: $\Psi_x = \frac{\partial \Psi_y}{\partial Y} = \Psi_z = 0$, $\frac{\partial \Theta}{\partial Y} \pm \mathrm{N_{rad}} Q_{\mathrm{rad}} = 0$;

at boundaries $Z = 0$ and $Z = 1$: $\Psi_x = \Psi_y = \frac{\partial \Psi_z}{\partial Z} = 0$, $\frac{\partial \Theta}{\partial Z} \pm \mathrm{N_{rad}} Q_{\mathrm{rad}} = 0$.

To determine the dimensionless radiation flux density Q_{rad}, we applied a method of solution with the use of effective radiation flux density [11, 13], which is based on realizing two difference equations with the use of a sequential overrelaxation method:

$$Q_{\mathrm{rad},k} = R_k - \sum_{i=1}^{N} F_{k-i} R_i, \tag{8}$$

$$R_k = (1-\varepsilon_k)\sum_{i=1}^{N} F_{k-i} R_i + \varepsilon_k (1-\xi)^4 \left(\Theta_k + 0.5\frac{1+\xi}{1-\xi}\right)^4. \tag{9}$$

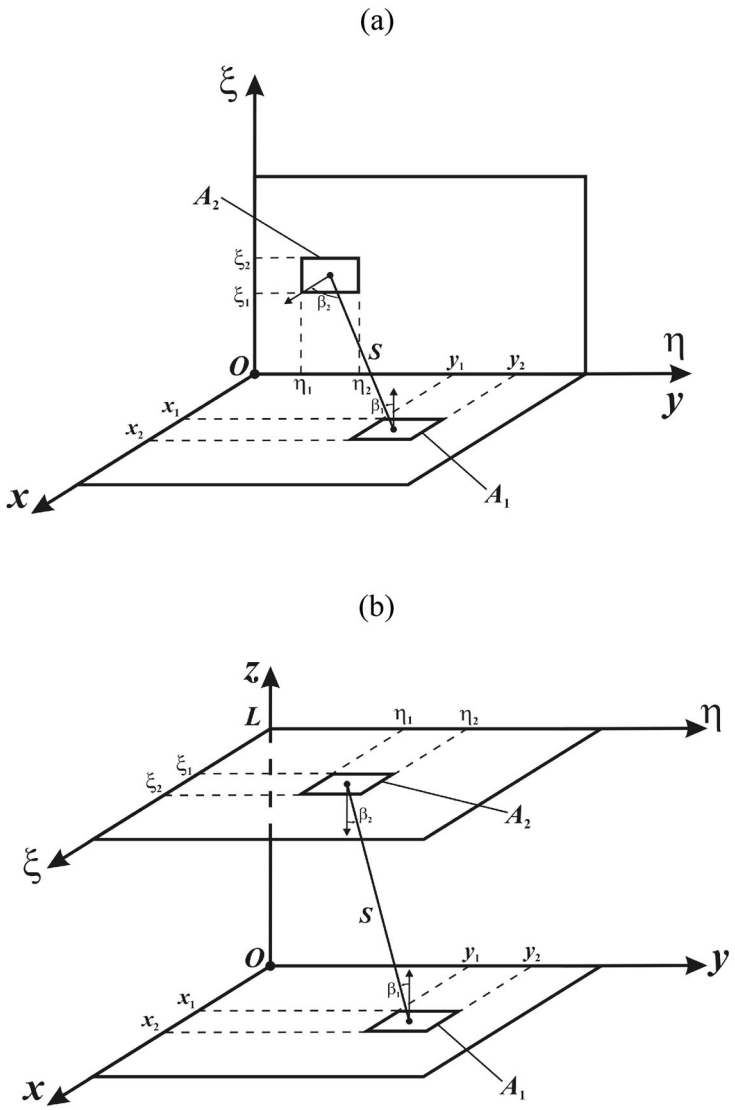

Fig. 2. A scheme of radiation heat exchange between perpendicular (a) and parallel (b) surfaces.

The view factors were calculated by definition [6, 11]:

$$F_{1-2} = \frac{1}{A_1} \int\limits_{A_1} \int\limits_{A_2} \frac{\cos\beta_1 \cos\beta_2}{\pi S^2} dA_2 dA_1,$$

which was expanded for the cubic enclosure (Fig. 2) as [6, 11]:

$$F_{1-2} = \frac{1}{(x_2 - x_1)(y_2 - y_1)} \sum_{l=1}^{2} \sum_{k=1}^{2} \sum_{j=1}^{2} \sum_{i=1}^{2} (-1)^{i+j+k+l} G(x_i, y_j, \eta_k, \xi_l).$$

In the case of orthogonal faces (Fig. 2a) [6, 11]:

$$G(x, y, \eta, \xi) = \frac{1}{2\pi} \left\{ (y - \eta) \sqrt{x^2 + \xi^2} \arctan \left[\frac{y - \eta}{\sqrt{x^2 + \xi^2}} \right] \right.$$
$$\left. - \frac{1}{4} \left[x^2 + \xi^2 - (y - \eta)^2 \right] \ln \left[x^2 + \xi^2 + (y - \eta)^2 \right] \right\},$$

and in the case of parallel faces (Fig. 2b) [6, 11]:

$$G(x,y,\eta,\xi)=\frac{1}{2\pi}\left\{(y-\eta)\sqrt{(x-\xi)^2+L^2}\cdot\arctan\left[\frac{y-\eta}{\sqrt{(x-\xi)^2+L^2}}\right]+(x-\xi)\right.$$
$$\left.\times\sqrt{(y-\eta)^2+L^2}\cdot\arctan\left[\frac{x-\xi}{\sqrt{(y-\eta)^2+L^2}}\right]-\frac{L^2}{2}\ln\left[(x-\xi)^2+(y-\eta)^2+L^2\right]\right\}.$$

To verify accuracy of the calculated view factors, we applied a very important property of the view factors, which follows from the energy conservation law. Radiation energy radiated from any surface k in a closed system is necessarily distributed over the other system surfaces in such a manner that the total energy incident on surfaces is equal to energy radiated from the surface k. From this it follows that $\sum_{i=1}^{N} F_{k-i}=1$.

The problem (1)–(9) with the corresponding boundary conditions was solved by a finite difference method [10, 12]. The applied method of solution was tested on the following model problems: 2D convection-radiation heat transfer in a square enclosure [13] and 3D thermal gravitational convection in a cube [10, 12]. Comparison of the results with those of other authors has revealed that the applied method yields quite good agreement.

ANALYSIS OF THE OBTAINED RESULTS

The calculations were performed with the following values of dimensionless complexes: $\mathrm{Ra}=10^3$, $\mathrm{N_{rad}}=16.79$; $\mathrm{Ra}=10^4$, $\mathrm{N_{rad}}=36.34$; $\mathrm{Ra}=10^5$, $\mathrm{N_{rad}}=77.87$; $\mathrm{Ra}=10^6$, $\mathrm{N_{rad}}=167.85$; $\mathrm{Pr}=0.7$; $\xi=0.97$; $0\le\tau\le100$; $0\le\varepsilon<1$.

Figure 3 represents motion trajectories of internal medium and temperature fields with $\varepsilon=0.6$, $\tau=100$, which correspond to different values of temperature difference. Regardless of the Rayleigh number value, a 3D convection structure is formed in the enclosure, which represents onset of upflows near the heated surface and downflows near the opposite cooled wall. The increase of the temperature difference results in narrowing along the vertical axis of the circulation region. We should note development of spiral motion of air masses from the side adiabatic walls toward the center of the enclosure. The observed vortex structures were earlier described in detail in conditions of the conjugate problem of thermal gravitational convection in a cubic enclosure with $\varepsilon=0$ [14, 15]. Consideration of surface radiation for nonconjugate heat transfer problems is evident, first of all, near adiabatic walls due to physical characteristics of this effect. Thermal radiation is received by the walls whose temperature changes as a result of this contact and this affects the motion intensity of the medium near these walls. The latter, due to the convective heat transfer mechanism leads to changes in thermal hydrodynamic parameters of the entire volume of the medium. We should note also that the influence of thermal radiation is mathematically described by boundary heat-insulation conditions that represent zero summarized density of heat fluxes due to radiation and thermal conductivity.

Figure 4 shows the influence of the presented surface emissivity of the walls on the flow structure and the temperature field inside the enclosure. An increase in ε has slight effect on configuration of the flow in the center of the enclosure. The most prominent changes are observed near the walls, one can see growing velocity of upflows and downflows, and also increasing amplitude of side spiral structures that characterize mass transfer from the vertical adiabatic walls. The temperature field also changes, one can observe decreasing temperature near the upper vertical horizontal wall and increasing temperature at the boundary $Z=0$.

We analyzed the influence of the Rayleigh number (Fig. 5) and the surface emissivity (Fig. 6) on average convection $\left(\mathrm{Nu_{conv}}=\int_0^1\int_0^1\left|\frac{\partial\Theta}{\partial X}\right|_{X=0}dYdZ\right)$ and radiation $\left(\mathrm{Nu_{rad}}=\mathrm{N_{rad}}\int_0^1\int_0^1 Q_{\mathrm{rad}}|_{X=0}\,dYdZ\right)$ Nusselt numbers on the vertical isothermal face $X=0$.

The growing temperature difference with $\varepsilon=0.6$ leads to intensification of convective and radiative heat transfer (Fig. 5). At $10^3\le\mathrm{Ra}\le10^5$ the influence of problem dimension on the integral convection

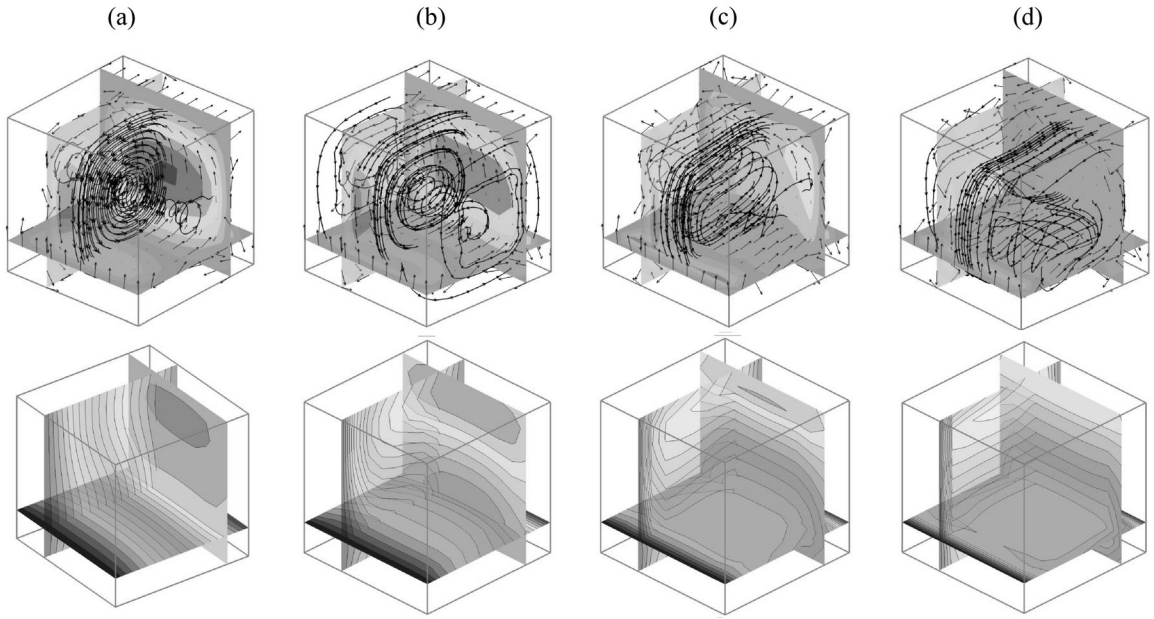

Fig. 3. Motion trajectories of medium and temperature fields for $\varepsilon = 0.6$, $\tau = 100$: $\mathrm{Ra} = 10^3$ (a), $\mathrm{Ra} = 10^4$ (b), $\mathrm{Ra} = 10^5$ (c), $\mathrm{Ra} = 10^6$ (d).

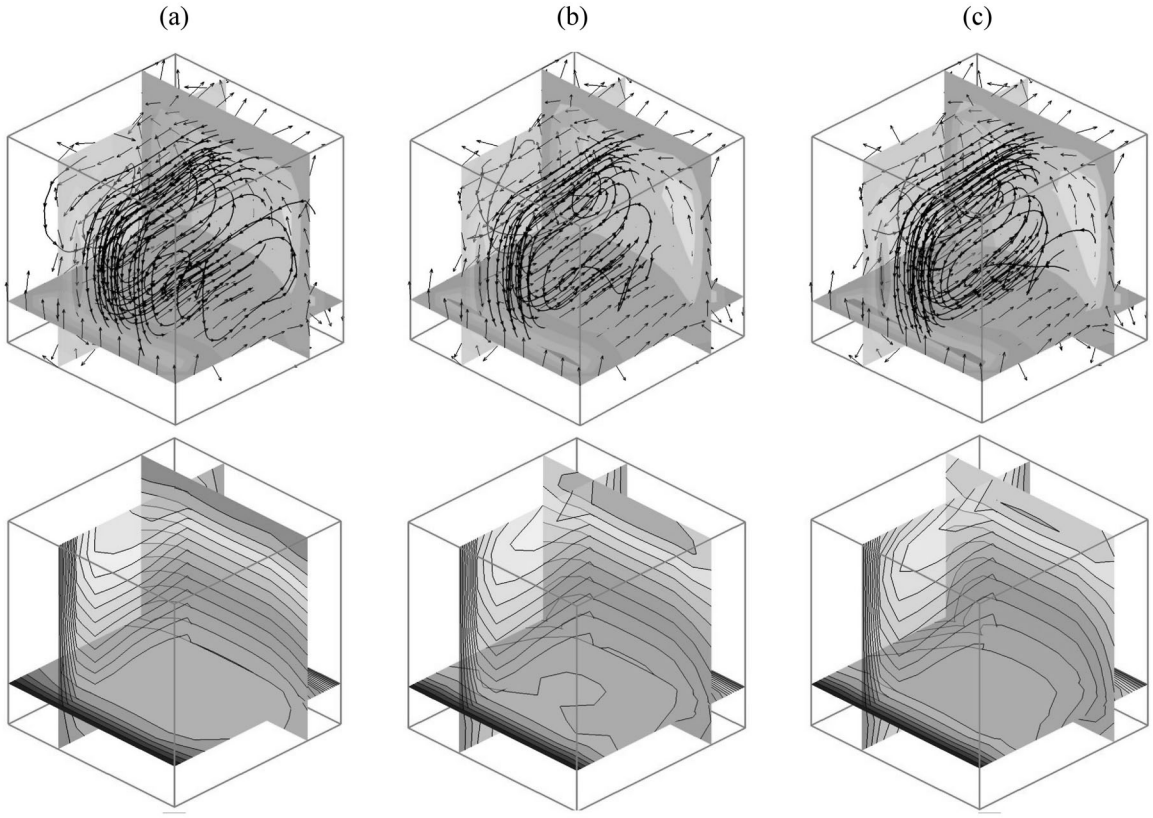

Fig. 4. Motion trajectories of medium and temperature fields for $\mathrm{Ra} = 10^5$, $\tau = 100$: $\varepsilon = 0$ (a), $\varepsilon = 0.3$ (b), $\varepsilon = 0.9$ (c).

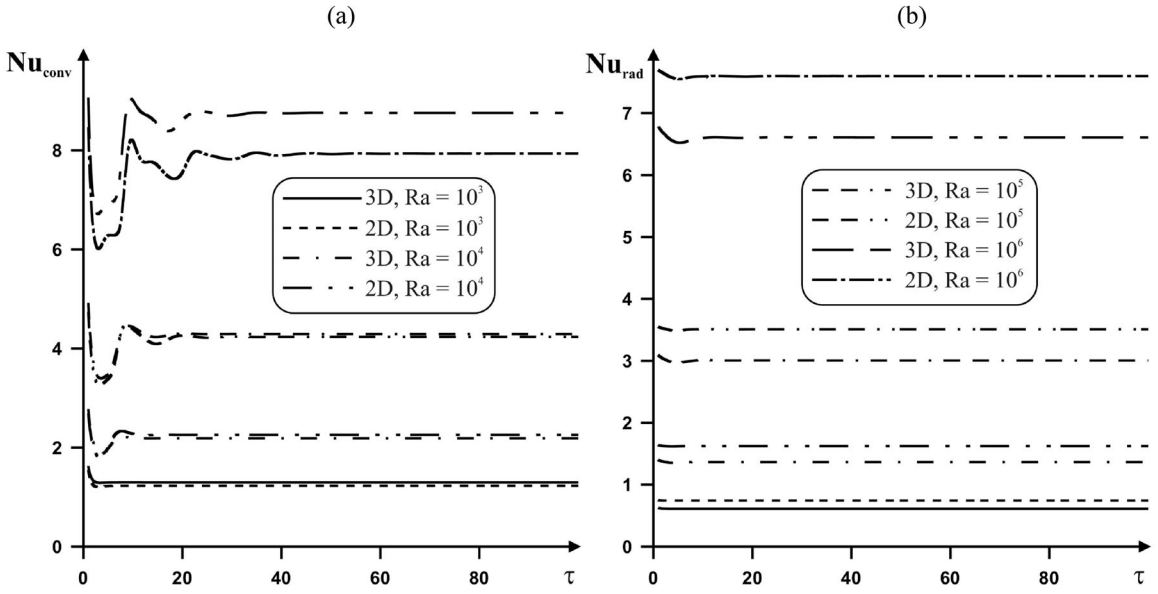

Fig. 5. Average Nusselt convection (a) and radiation (b) numbers versus time, problem dimension, and Rayleigh number for $\varepsilon = 0.6$.

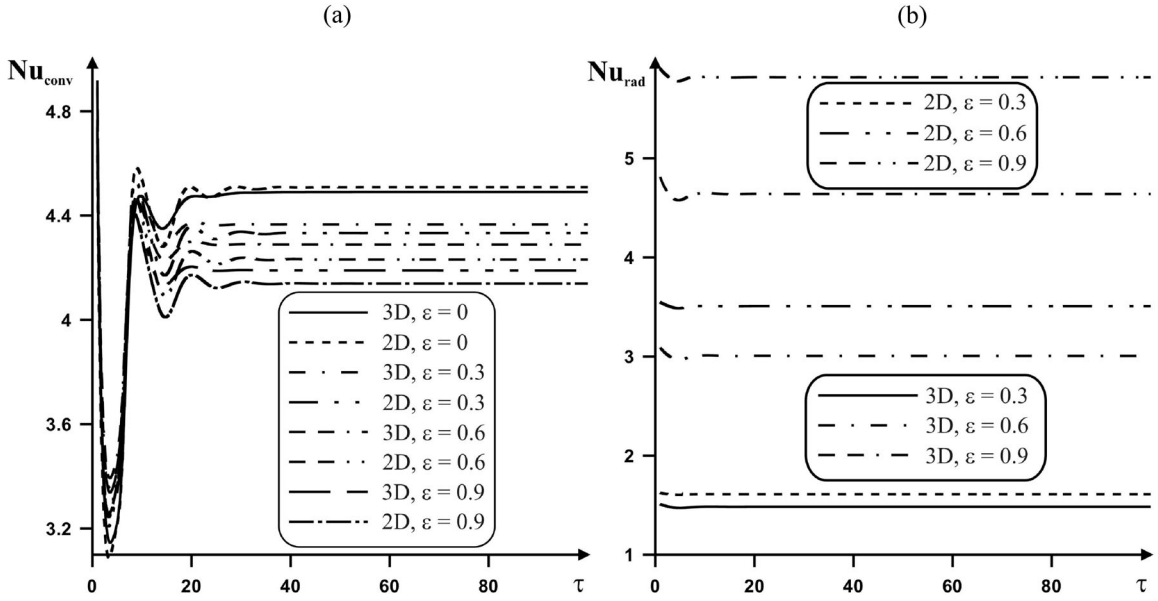

Fig. 6. Average Nusselt convection (a) and radiation (b) numbers versus time, problem dimension, and surface emissivity at $\mathrm{Ra} = 10^5$.

coefficient of heat transfer is insignificant (Fig. 5a), whereas the Nusselt radiation number, with regard to the third coordinate, decreases (Fig. 5b). At high Rayleigh numbers ($\mathrm{Ra} \geq 10^6$), there is observed considerable influence of the problem dimension: $\mathrm{Nu_{conv}}$ grows, while $\mathrm{Nu_{rad}}$ decreases when passing from 2D problem to 3D problem.

The influence of time on the process analyzed manifests itself in formation of an initial nonstationary stage for an average Nusselt convection number. Growth of Ra leads to increasing time of $\mathrm{Nu_{conv}}$ onset, at that, the time of onset of the integral convection heat exchange coefficient does not depend on problem dimension. For $\mathrm{Nu_{rad}}$, nonstationarity appears only at $\mathrm{Ra} = 10^6$.

Growth of the surface emissivity regardless of the problem dimension leads to increasing average

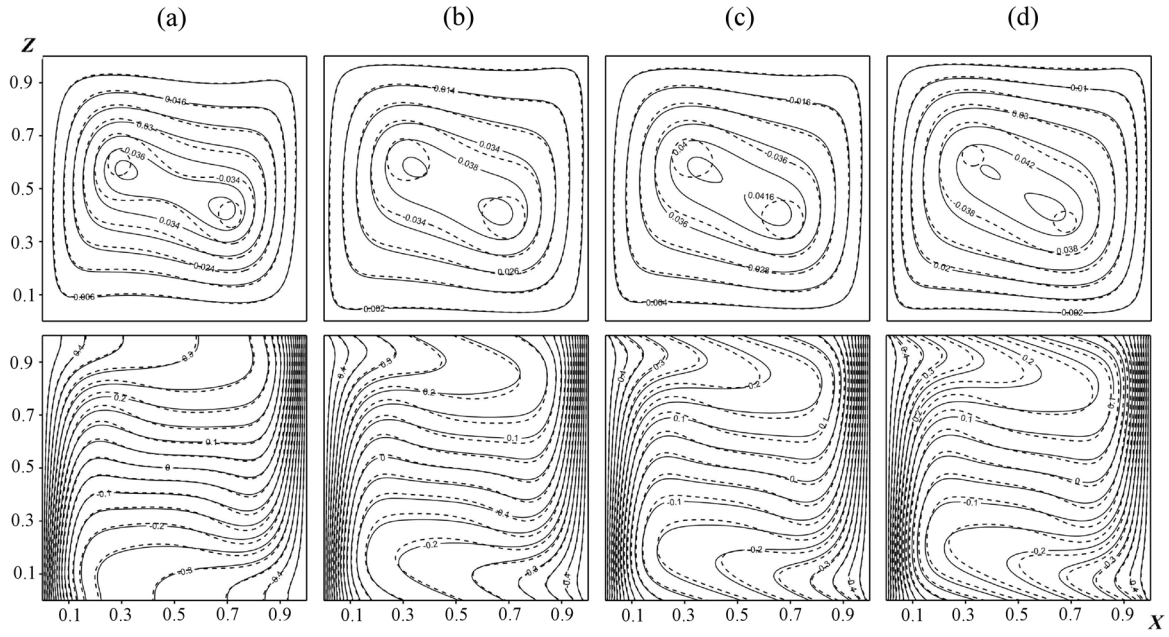

Fig. 7. Isolines of y-component of vector potential and temperature in 3D case (—) and stream function and temperature in 2D case (- - -) at $\mathrm{Ra} = 10^5$, $\tau = 100$: $\varepsilon = 0$ (a), $\varepsilon = 0.3$ (b), $\varepsilon = 0.6$ (c), $\varepsilon = 0.9$ (d).

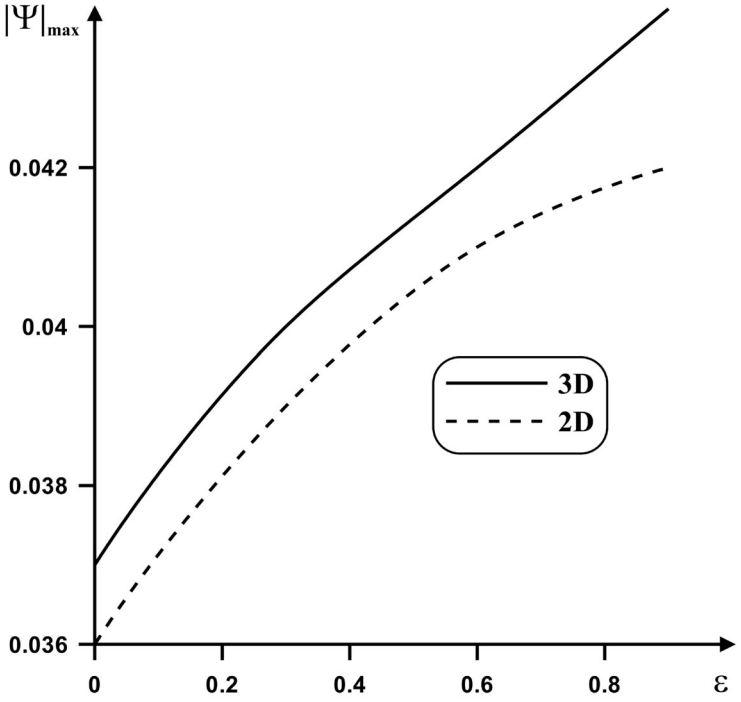

Fig. 8. Maximum absolute value of stream function versus surface emissivity and problem dimension at $\mathrm{Ra} = 10^5$, $\tau = 100$.

Nusselt radiation number (Fig. 6b). At that, $\mathrm{Nu}_{\mathrm{conv}}$ behavior is nonmonotonic: at $\mathrm{Ra} = 10^3$ an increase in ε leads to a growth of $\mathrm{Nu}_{\mathrm{conv}}$; at $\mathrm{Ra} = 10^4$, a change in the surface emissivity in the range from 0 to 0.6 results in increasing $\mathrm{Nu}_{\mathrm{conv}}$, and at $\varepsilon > 0.6$ there is observed a decrease in the integral convection heat exchange coefficient; at $\mathrm{Ra} \geq 10^5$, $\mathrm{Nu}_{\mathrm{conv}}$ decreases over the entire range of ε. The noticed features for $\mathrm{Nu}_{\mathrm{conv}}$ are observed regardless of the problem dimension. The influence of considering the third coordinate is similar to Fig. 5, and this variation becomes more considerable as the surface emissivity grows, particularly, for average Nusselt radiation number.

Figure 7 represents comparison of both the isolines of stream function (for 2D problem) and Ψ_y component of vector potential (for 3D problem at the section $Y = 0.5$) and the isotherms for two statements of the problem with different values of the surface emissivity. Over the entire range of ε, we observe some distinctions in the structure of the central part of isolines of stream function and y-component of vector potential. The level of these distinctions grows with the surface emissivity, which is most evident in the distribution of isotherms.

Figure 8 shows growing convective flow intensity with regard to the third coordinate.

As a result of our investigations we obtained approximation relationships for average radiation ($\mathrm{Nu_{rad}}$) and total ($\mathrm{Nu_{rad}}$) ($\mathrm{Nu_{total}} = \mathrm{Nu_{conv}} + \mathrm{Nu_{rad}}$) Nusselt numbers on the vertical isothermal face at $10^3 \le \mathrm{Ra} \le 10^6$, $\mathrm{Pr} = 0.7$, and $0.3 \le \varepsilon \le 0.9$:

$$\mathrm{Nu}^{2D}_{rad} = 0.135 \cdot \mathrm{Ra}^{0.336} \cdot \varepsilon^{1.16}, \qquad \mathrm{Nu}^{3D}_{rad} = 0.098 \cdot \mathrm{Ra}^{0.344} \cdot \varepsilon^{1.027},$$

and

$$\mathrm{Nu}^{2D}_{total} = 0.324 \cdot \mathrm{Ra}^{0.3} \cdot \varepsilon^{0.455} \qquad \mathrm{Nu}^{3D}_{total} = 0.275 \cdot \mathrm{Ra}^{0.305} \cdot \varepsilon^{0.362}.$$

CONCLUSIONS

The numerical analysis of convection-radiation heat transfer in a cubic enclosure was performed in a wide range of key parameters: $10^3 \le \mathrm{Ra} \le 10^6$, $0 \le \varepsilon \le 0.9$, and $0 \le \tau \le 100$. As a result, we have obtained distributions of isolines of the y-component of the vector potential and temperature, and also 3D motion trajectories of the medium, velocity and temperature fields. The influence of the Rayleigh number, surface emissivity, and dimensionless time on local and integral characteristics of the process were analyzed in detail. Considerable influence of problem dimension at $\mathrm{Ra} \ge 10^6$ has been observed: $\mathrm{Nu_{conv}}$ increases and $\mathrm{Nu_{rad}}$ decreases when passing from the 2D problem to the 3D problem. It has been shown that growth of the surface emissivity regardless of the Rayleigh number value and the problem dimension results in increasing average Nusselt radiation number, whereas the integral Nusselt radiation number changes nonmonotonically. Also, it has been shown that the most prominent distinctions in the structure of the core of local process parameters are attained at high values of Ra and ε. We have found approximation relationships for average radiation and total Nusselt numbers as a function of Rayleigh number, surface emissivity, and problem dimension.

ACKNOWLEDGMENTS

This work was supported by the Tomsk State University Academic Fund Program, and by the Russian Foundation for Basic Research, grant no. 14-08-31137 mol_a.

NOTATIONS

a—thermal diffusivity coefficient, $\mathrm{m^2/s}$

F_{k-i}—view factors between kth and ith surfaces

g_z—gravitational acceleration component projected onto the z axis, $\mathrm{m/s^2}$

k—heat conductivity coefficient of diathermal medium, $\mathrm{W/(m{\cdot}K)}$

L—size of solution domain, m

N—the number of partition surfaces

$\mathrm{N_{rad}} = \sigma T_\mathrm{h}^4 L/[k(T_\mathrm{h} - T_\mathrm{c})]$—radiation parameter

$\mathrm{Pr} = \nu/a$—Prandtl number

Q_rad—dimensionless radiation flux density

$Q_{\mathrm{rad},k}$—dimensionless density of radiation flux supplied to the kth surface

R_k—dimensionless density of effective radiation of the kth surface

$\mathrm{Ra} = g_z \beta (T_\mathrm{h} - T_\mathrm{c}) L^3/(\nu a)$—Rayleigh number

t—time, s

t_0—time scale, s

T—temperature, K

$T_0 = 0.5(T_\mathrm{h} + T_\mathrm{c})$—initial temperature in the solution domain, K

T_c—temperature at the boundary $x = L$, K

T_h—temperature at the boundary $x = 0$, K

u, v, w—velocity components projected onto x, y, z axes, respectively, m/s

U, V, W—dimensionless velocities corresponding to velocities u, v, w

V_0—velocity scale (convection velocity), m/s

x, y, z—coordinates of Cartesian coordinate system, m

X, Y, Z—dimensionless coordinates corresponding to x, y, z coordinates

β—temperature coefficient of volumetric expansion, 1/K

ε—surface emissivity of the wall

ε_k—surface emissivity of the kth surface

Θ—dimensionless temperature

Θ_k—dimensionless temperature of the kth surface

λ—radiation wavelength, m

ν—kinematic viscosity coefficient, m^2/s

$\xi = T_\mathrm{c}/T_\mathrm{h}$—temperature parameter

σ—Stephan–Boltzmann constant, $\mathrm{W}/(\mathrm{m}^2 \cdot \mathrm{K}^4)$

τ—dimensionless time

τ_λ—optical thickness of the medium

ψ_x, ψ_y, ψ_z—vector potential components in Cartesian coordinate system, m^2/s

ψ_0—scale of vector potential component, m^2/s

Ψ_x, Ψ_y, Ψ_z—dimensionless components of vector potential, corresponding to ψ_x, ψ_y, ψ_z

ω_x, ω_y, ω_z—components of vorticity vector in Cartesian coordinate system, 1/s

ω_0—scale of vorticity vector components, 1/s

Ω_x, Ω_y, Ω_z—dimensionless components of vorticity vector, corresponding to ω_x, ω_y, ω_z

Indices

c—cooled surface

h—heated surface

i, k—surface number

rad—radiation

REFERENCES

1. Steinberg, D.S., *Cooling Techniques for Electronic Equipment*, New York: Wiley, 1991.
2. Kuznetsov, G.V. and Sheremet, M.A., New Approach to the Mathematical Modeling of Thermal Regimes for Electronic Equipment, *Russ. Microel.*, 2008, vol. 37, no. 2, pp. 131–138.
3. Akiyama, M. and Chong, Q.P., Numerical Analysis of Natural Convection with Surface Radiation in a Square Enclosure, *Num. Heat Transfer*, pt. A, 1997, vol. 31, pp. 419–433.
4. Wang, H., Xin, S., and Le Quere, P., Numerical Study of Natural Convection-Surface Radiation Coupling in Air-Filled Square Cavities, *C.R. Mecanique*, 2006, vol. 334, pp. 48–57.
5. Colomer, G., Costa, M., Consul, R., and Oliva, A., Three-Dimensional Numerical Simulation of Convection and Radiation in a Differentially Heated Cavity Using the Discrete Ordinates Method, *Int. J. Heat Mass Transfer*, 2004, vol. 47, pp. 257–269.
6. Albanakis, C. and Bouris, D., 3D Conjugate Heat Transfer with Thermal Radiation in a Hollow Cube Exposed to External Flow, *Int. J. Heat Mass Transfer*, 2008, vol. 51, pp. 6157–6168.
7. Kolsi, L., Abidi, A., Maatki, C., Borjini, M.N., and Ben Aissia, H., Combined Radiation-Natural Convection in Three-Dimensional Verticals Cavities, *Thermal Sci.*, 2011, vol. 15, pp. 327–339.
8. Lei, C. and Patterson, J.C., A Direct Three-Dimensional Simulation of Radiation-Induced Natural Convection in a Shallow Wedge, *Int. J. Heat Mass Transfer*, 2003, vol. 46, pp. 1183–1197.
9. Lei, C. and Patterson, J.C., Natural Convection in a Reservoir Sidearm Subject to Solar Radiation: Experimental Observations, *Exp. Fluids*, 2002, vol. 32, pp. 590–599.
10. Kuznetsov, G.V. and Sheremet, M.A., Conjugate Natural Convection with Radiation in an Enclosure, *Int. J. Heat Mass Transfer*, 2009, vol. 52, pp. 2215–2223.
11. Siegel, R. and Howell, J.R., *Thermal Radiation Heat Transfer*, London: Taylor & Francis, 2002.
12. Kuznetsov, G.V. and Sheremet, M.A., A Numerical Simulation of Double-Diffusive Conjugate Natural Convection in an Enclosure, *Int. J. Therm. Sci.*, 2011, vol. 50, pp. 1878–1886.
13. Martyushev, S.G. and Sheremet, M.A., Numerical Analysis of Conjugate Natural Convection and Surface Radiation in an Enclosure with Local Heat Source, *Comput. Therm. Sci.*, 2013, vol. 5, pp. 267–287.
14. Sheremet, M.A., Spatial Regimes of Conjugate Natural Convection in a Cubic Enclosure, *Vestnik Tomsk. Gos. Univ., Mat. Mekh.*, 2012, no. 1(17), pp. 119–126.
15. Sheremet, M.A., Mathematical Simulation of Nonstationary Regimes of Natural Convection in a Cubical Enclosure with Finite-Thickness Heat-Conducting Walls, *J. Eng. Therm.*, 2013, vol. 22, no. 4, pp. 298-308.